have reported findings that support the idea that reticular pseudodrusen may represent choroidal changes. Sohrab and associates[18] reported that correlation of registered IR, FAF, and red-free images localized the reticular pattern to the intravascular choroidal stroma on en face OCT sections. Querques and associates[17] showed that the reticular patterns appeared as hypofluorescent lesions on IA, closely abutting but not overlying the large choroidal vessels. Thus, although further investigations are necessary to determine the exact origin of reticular pseudodrusen, choroidal involvement should be taken into consideration to its pathogenesis.

Several studies have reported the abnormalities in the choroidal vascular structure in eyes with reticular pseudodrusen. A histologic report showed that small choroidal blood vessels were almost absent and larger vessels were also decreased in an eye with reticular pseudodrusen.[2] Another histologic report showed patchy loss of choroidal capillaries and a thin choroid in a pathologic specimen of reticular pseudodrusen.[4] In the current study, en face high-penetration SS-OCT images revealed that the choroidal vascular area of the Haller layer was decreased in eyes with reticular pseudodrusen but without CNV or geographic atrophy, compared with normal eyes. Taken together, our in vivo findings and previous histopathology data suggest that there may be a diffuse loss of small and large choroidal vessels, including choroidal capillaries, in eyes with reticular pseudodrusen, leading to choroidal thinning and reduced volume in the whole macular area prior to the development of CNV or geographic atrophy. Although choroidal thinning or reduced choroidal volume does not necessarily imply choroidal ischemia, these results suggest that atrophy of the whole choroid may be involved in the occurrence or development of reticular pseudodrusen. The reduction of ischemic factors, such as reducing cholesterol/triglyceride levels, controlling blood pressure, and taking anticoagulant agents, may be a therapeutic strategy for slowing choroidal atrophy and ultimately reducing the risk for late AMD in patients with reticular pseudodrusen. Further studies are necessary to evaluate the relationship between the progression to late AMD, systemic diseases, and reticular pseudodrusen.

There are several limitations of this study. Although high-penetration SS-OCT increases the sensitivity of the choroid, light is still scattered by the RPE and choroid, which makes visualization of the chorioscleral interface difficult in a few images. In the current study, in B-scans where it was difficult to identify the whole outer choroid, 7-15 points where the chorioscleral interface could be identified were chosen and connected to create a segmentation line. There was no automated segmentation software available for measuring choroidal thickness for the SS-OCT prototype system; thus, all segmentations were performed manually. However, we have previously shown good interobserver repeatability with this technique.[28] Because this was a cross-sectional study, we might have overlooked stage 4 reticular pseudodrusen (fading of the subretinal material because of reabsorption and migration within the inner retinal layers).[40] Recently, using multimodal imaging, Spaide[41] demonstrated that eyes with regression of reticular pseudodrusen develop outer retinal atrophy and loss of the underlying choroidal thickness. Thus, further assessment is necessary to evaluate the choroidal changes in stage 4 of reticular pseudodrusen.

In conclusion, our study revealed that macular choroidal thickness and volume in eyes with reticular pseudodrusen were significantly decreased, regardless of CNV or geographic atrophy. Furthermore, en face SS-OCT images showed that the choroidal vascular area was decreased in eyes with reticular pseudodrusen. Although it remains unknown whether choroidal thinning and choroidal vascular changes are causes or consequences of reticular pseudodrusen, the findings of this study may help to elucidate its pathogenesis. In the future, we hope to perform longitudinal studies using SS-OCT to further elucidate the involvement of the choroid in the pathogenesis of reticular pseudodrusen.

ALL AUTHORS HAVE COMPLETED AND SUBMITTED THE ICMJE FORM FOR DISCLOSURE OF POTENTIAL CONFLICTS OF INTEREST. Financial disclosures: Nagahisa Yoshimura: advisory board of Topcon. This research was supported in part by the Grant-in-Aid for Scientific Research (21791679) from the Japan Society for the Promotion of Science (JSPS) and Topcon. Author contributions: conception and design (N.U.A., S.O.); analysis and interpretation (N.U.A., S.O.); writing the article (N.U.A., S.O.); critical revision of the article (S.O., N.Y.); final approval of the article (N.U.A., S.O., A.A.E., A.Takahashi, A.O., H.T., K.Y., A.Tsujikawa, N.Y.); data collection (N.U.A., A.A.E., A.Takahashi); provision of materials (S.O., A.O., H.T., K.Y., A.Tsujikawa., N.Y.); statistical expertise (N.U.A., S.O.); obtaining funding (S.O.); literature search (N.U.A., S.O.).

REFERENCES

1. Mimoun G, Soubrane G, Coscas G. Macular drusen. *J Fr Ophthalmol* 1990;13(10):511–530.
2. Arnold JJ, Sarks SH, Killingsworth MC, Sarks JP. Reticular pseudodrusen. A risk factor in age-related maculopathy. *Retina* 1995;15(3):183–191.
3. Cohen SY, Dubois L, Tadayoni R, Delahaye-Mazza C, Debibie C, Quentel G. Prevalence of reticular pseudodrusen in age-related macular degeneration with newly diagnosed choroidal neovascularisation. *Br J Ophthalmol* 2007;91(3):354–359.
4. Sarks J, Arnold J, Ho IV, Sarks S, Killingsworth M. Evolution of reticular pseudodrusen. *Br J Ophthalmol* 2011;95(7):979–985.
5. Pumariega NM, Smith RT, Sohrab MA, Letien V, Souied EH. A prospective study of reticular macular disease. *Ophthalmology* 2011;118(8):1619–1625.
6. Schmitz-Valckenberg S, Alten F, Steinberg JS, et al. Reticular drusen associated with geographic atrophy in age-related

macular degeneration. *Invest Ophthalmol Vis Sci* 2011;52(9): 5009–5015.
7. Klein R, Meuer SM, Knudtson MD, Iyengar SK, Klein BE. The epidemiology of retinal reticular drusen. *Am J Ophthalmol* 2008;145(2):317–326.
8. Ueda-Arakawa N, Ooto S, Nakata I, et al. Prevalence and genomic association of reticular pseudodrusen in age-related macular degeneration. *Am J Ophthalmol* 2013;155(2): 260–269.e2.
9. Zweifel SA, Imamura Y, Spaide TC, Fujiwara T, Spaide RF. Prevalence and significance of subretinal drusenoid deposits (reticular pseudodrusen) in age-related macular degeneration. *Ophthalmology* 2010;117(9):1775–1781.
10. Lee MY, Yoon J, Ham DI. Clinical characteristics of reticular pseudodrusen in Korean patients. *Am J Ophthalmol* 2012; 153(3):530–535.
11. Lee MY, Yoon J, Ham DI. Clinical features of reticular pseudodrusen according to the fundus distribution. *Br J Ophthalmol* 2012;96(9):1222–1226.
12. Querques G, Massamba N, Srour M, Boulanger E, Georges A, Souied EH. Impact of reticular pseudodrusen on macular function. *Retina* 2014;34(2):321–329.
13. Ooto S, Ellabban AA, Ueda-Arakawa N, et al. Reduction of retinal sensitivity in eyes with reticular pseudodrusen. *Am J Ophthalmol* 2013;156(6):1184–1191.e2.
14. Smith RT, Sohrab MA, Busuoic M, Barile G. Reticular macular disease. *Am J Ophthalmol* 2009;148(5):733–743.e2.
15. Spaide RF, Curcio CA. Drusen characterization with multimodal imaging. *Retina* 2010;30(9):1441–1454.
16. Ueda-Arakawa N, Ooto S, Tsujikawa A, Yamashiro K, Oishi A, Yoshimura N. Sensitivity and specificity of detecting reticular pseudodrusen in multimodal imaging in Japanese patients. *Retina* 2013;33(3):490–497.
17. Querques G, Querques L, Forte R, Massamba N, Coscas F, Souied EH. Choroidal changes associated with reticular pseudodrusen. *Invest Ophthalmol Vis Sci* 2012;53(3):1258–1263.
18. Sohrab MA, Smith RT, Salehi-Had H, Sadda SR, Fawzi AA. Image registration and multimodal imaging of reticular pseudodrusen. *Invest Ophthalmol Vis Sci* 2011;52(8):5743–5748.
19. Spaide RF, Koizumi H, Pozonni MC. Enhanced depth imaging spectral-domain optical coherence tomography. *Am J Ophthalmol* 2008;146(4):496–500.
20. Margolis R, Spaide RF. A pilot study of enhanced depth imaging optical coherence tomography of the choroid in normal eyes. *Am J Ophthalmol* 2009;147(5):811–815.
21. Imamura Y, Fujiwara T, Margolis R, Spaide RF. Enhanced depth imaging optical coherence tomography of the choroid in central serous chorioretinopathy. *Retina* 2009;29(10):1469–1473.
22. Fujiwara T, Imamura Y, Margolis R, et al. Enhanced depth imaging optical coherence tomography of the choroid in highly myopic eyes. *Am J Ophthalmol* 2009;148(3):445–450.
23. Manjunath V, Goren J, Fujimoto JG, Duker JS. Analysis of choroidal thickness in age-related macular degeneration using spectral-domain optical coherence tomography. *Am J Ophthalmol* 2011;152(4):663–668.
24. Chung SE, Kang SW, Lee JH, Kim YT. Choroidal thickness in polypoidal choroidal vasculopathy and exudative age-related macular degeneration. *Ophthalmology* 2011;118(5): 840–845.
25. Jirarattanasopa P, Ooto S, Nakata I. Choroidal thickness, vascular hyperpermeability, and complement factor H in age-related macular degeneration and polypoidal choroidal vasculopathy. *Invest Ophthalmol Vis Sci* 2012;53(7):3663–3672.
26. Switzer DJ Jr, Mendonça LS, Saito M, et al. Segregation of ophthalmoscopic characteristics according to choroidal thickness in patients with early age-related macular degeneration. *Retina* 2012;32(7):1265–1271.
27. de Bruin DM, Burnes DL, Loewenstein J, et al. In vivo three-dimensional imaging of neovascular age-related macular degeneration using optical frequency domain imaging at 1050 nm. *Invest Ophthalmol Vis Sci* 2008;49(10):4545–4552.
28. Hirata M, Tsujikawa A, Matsumoto A, et al. Macular choroidal thickness and volume in normal subjects measured by swept-source optical coherence tomography. *Invest Ophthalmol Vis Sci* 2011;52(8):4971–4978.
29. Keane P, Ruiz-Garcia H, Sadda S. Clinical applications of long-wavelength (1,000-nm) optical coherence tomography. *Ophthalmic Surg Lasers Imaging* 2011;42(suppl):S67–S74.
30. Jirarattanasopa P, Ooto S, Tsujikawa A, et al. Assessment of macular choroidal thickness by optical coherence tomography and angiographic changes in central serous chorioretinopathy. *Ophthalmology* 2012;119(8):1666–1678.
31. Spaide RF. Age-related choroidal atrophy. *Am J Ophthalmol* 2009;147(5):801–810.
32. Ellabban AA, Tsujikawa A, Matsumoto A, et al. Three-dimensional tomographic features of dome-shaped macula by swept-source optical coherence tomography. *Am J Ophthalmol* 2013;155(2):320–328.e2.
33. Ellabban AA, Tsujikawa A, Matsumoto A, et al. Macular choroidal thickness and volume in eyes with angioid streaks measured by swept source optical coherence tomography. *Am J Ophthalmol* 2012;153(6):1133–1143.
34. Ellabban AA, Tsujikawa A, Matsumoto A, et al. Macular choroidal thickness measured by swept source optical coherence tomography in eyes with inferior posterior staphyloma. *Invest Ophthalmol Vis Sci* 2012;53(12):7735–7745.
35. Ellabban AA, Tsujikawa A, Ooto S, et al. Focal choroidal excavation in eyes with central serous chorioretinopathy. *Am J Ophthalmol* 2013;156(4):673–683.e1.
36. Ikuno Y, Kawaguchi K, Nouchi T, Yasuno Y. Choroidal thickness in healthy Japanese subjects. *Invest Ophthalmol Vis Sci* 2010;51(4):2173–2176.
37. Zweifel SA, Spaide RF, Curcio CA, Malek G, Imaura Y. Reticular pseudodrusen are subretinal drusenoid deposits. *Ophthalmology* 2010;117(2):303–312.e1.
38. Curcio CA, Messinger JD, Sloan KR, McGwin G, Medeiros NE, Spaide RF. Subretinal drusenoid deposits in non-neovascular age-related macular degeneration: morphology, prevalence, topography, and biogenesis model. *Retina* 2013;33(2):265–276.
39. Schmitz-Valckenberg S, Steinberg JS, Fleckenstein M, Visvalingam S, Brinkmann CK, Holz FG. Combined confocal scanning laser ophthalmoscopy and spectral-domain optical coherence tomography imaging of reticular drusen associated with age-related macular degeneration. *Ophthalmology* 2010; 117(6):1169–1176.
40. Querques G, Canouï-Poitrine F, Coscas F, et al. Analysis of progression of reticular pseudodrusen by spectral domain–optical coherence tomography. *Invest Ophthalmol Vis Sci* 2012;53(3):1264–1270.
41. Spaide RF. Outer retinal atrophy after regression of subretinal drusenoid deposits as newly recognized form of late age-related macular degeneration. *Retina* 2013;33(9):1800–1808.

Biosketch

Naoko Ueda-Arakawa, MD, graduated from Kyoto University, Faculty of Medicine. She completed her residency program at Kyoto University Hospital and a fellowship at Osaka Red Cross Hospital, Osaka, Japan. She is now in a PhD program in the Department of Ophthalmology and Visual Sciences at Kyoto University under the supervisor of Professor Nagahisa Yoshimura. Her main interest is imaging analysis of macular diseases.

SUPPLEMENTARY TABLE 1. Comparison of Mean Age and Axial Length of Eyes With Reticular Pseudodrusen Among 3 Subgroups

	Group 1[a] (n = 20)	Group 2[a] (n = 10)	Group 3[a] (n = 8)	P^b	P^c	P^d	P^e
Mean age	77.6 ± 6.0	81.8 ± 7.9	81.1 ± 5.9	.183	.218	.389	.973
Mean axial length (mm)	23.2 ± 0.9	23.6 ± 0.7	23.8 ± 1.2	.268	.503	.296	.910

All values are presented as mean ± standard deviation.

[a]Group 1: eyes with reticular pseudodrusen and without late age-related macular degeneration (AMD); Group 2: eyes with reticular pseudodrusen and exudative AMD; Group 3: eyes with reticular pseudodrusen and geographic atrophy.

[b]Comparison between the 3 subgroups by 1-way analysis of variance.

[c]Comparison between Group 1 and Group 2 by the Tukey-Kramer test.

[d]Comparison between Group 1 and Group 3 by the Tukey-Kramer test.

[e]Comparison between Group 2 and Group 3 by the Tukey-Kramer test.

SUPPLEMENTARY TABLE 2. Comparison of Mean Choroidal Thickness and Volume of Eyes With Reticular Pseudodrusen Among 3 Subgroups

	Mean Choroidal Thickness (μm)			Mean Choroidal Volume (mm^3)						
Area[a]	Group 1[b] (n = 20)	Group 2[b] (n = 10)	Group 3[b] (n = 8)	Group 1[b] (n = 20)	Group 2[b] (n = 10)	Group 3[b] (n = 8)	P^c	P^d	P^e	P^f
Center	138.1 ± 52.2	148.0 ± 53.1	151.2 ± 45.9	0.11 ± 0.04	0.12 ± 0.04	0.12 ± 0.04	.787	.871	.811	.990
Inner temporal	145.9 ± 49.7	149.6 ± 47.1	162.6 ± 44.0	0.23 ± 0.08	0.23 ± 0.07	0.26 ± 0.07	.708	.979	.681	.832
Inner superior	138.8 ± 54.3	145.5 ± 46.4	155.0 ± 36.1	0.22 ± 0.09	0.23 ± 0.07	0.24 ± 0.06	.731	.934	.708	.910
Inner nasal	121.2 ± 49.2	130.9 ± 53.4	139.0 ± 34.5	0.19 ± 0.08	0.21 ± 0.08	0.22 ± 0.05	.654	.857	.646	.932
Inner inferior	129.2 ± 49.0	141.0 ± 61.7	147.7 ± 45.3	0.20 ± 0.08	0.22 ± 0.10	0.23 ± 0.07	.662	.827	.671	.959
Outer temporal	140.7 ± 39.2	144.9 ± 43.9	159.2 ± 38.4	0.75 ± 0.21	0.77 ± 0.23	0.84 ± 0.20	.552	.960	.516	.733
Outer superior	139.2 ± 44.8	139.6 ± 46.6	153.4 ± 35.9	0.74 ± 0.24	0.74 ± 0.25	0.81 ± 0.19	.721	1.000	.713	.781
Outer nasal	101.0 ± 36.6	107.5 ± 42.4	117.7 ± 22.9	0.53 ± 0.19	0.57 ± 0.22	0.62 ± 0.12	.539	.883	.507	.820
Outer inferior	130.4 ± 38.6	141.8 ± 62.4	143.6 ± 28.1	0.69 ± 0.20	0.75 ± 0.33	0.76 ± 0.15	.700	.781	.753	.996
Whole macula	129.3 ± 40.6	135.8 ± 46.3	145.4 ± 30.8	3.66 ± 1.15	3.84 ± 1.31	4.11 ± 0.87	.635	.910	.607	.868

All values are presented as mean ± standard deviation.

[a]Center = within 0.5 mm from the foveal center; Inner = 0.5–1.5 mm from the foveal center; Outer = 1.5–3.0 mm from the foveal center; Whole = within 3.0 mm from the foveal center.

[b]Group 1: eyes with reticular pseudodrusen and without late age-related macular degeneration (AMD); Group 2: eyes with reticular pseudodrusen and exudative AMD; Group 3: eyes with reticular pseudodrusen and geographic atrophy.

[c]Comparison between the 3 subgroups by 1-way analysis of variance.

[d]Comparison between Group 1 and Group 2 by the Tukey-Kramer test.

[e]Comparison between Group 1 and Group 3 by the Tukey-Kramer test.

[f]Comparison between Group 2 and Group 3 by the Tukey-Kramer test.

SUPPLEMENTARY TABLE 3. Comparison of Mean Choroidal Thickness in Each ETDRS Sector; 20 Eyes With Reticular Pseudodrusen Without Late Age-Related Macular Degeneration (Group 1) Were Grouped Into 2 Subgroups According to Whether Reticular Pseudodrusen Covered More or Less Than Half of Each Area

	Reticular Pseudodrusen Covered More Than Half of the Area		Reticular Pseudodrusen Covered Less Than Half of the Area		
Area[a]	Mean Choroidal Thickness (μm)	Number of Eyes	Mean Choroidal Thickness (μm)	Number of Eyes	*P*[b]
Center	125.1 ± 26.5	8	146.7 ± 63.8	12	.700
Inner temporal	141.1 ± 31.6	16	165.5 ± 100.2	4	.925
Inner superior	140.7 ± 57.0	18	122.0 ± 8.8	2	.529
Inner nasal	131.6 ± 55.9	13	101.9 ± 27.5	7	.322
Inner inferior	129.5 ± 34.2	13	128.7 ± 72.5	7	.191
Outer temporal	141.6 ± 20.5	13	138.9 ± 63.4	7	.122
Outer superior	141.6 ± 44.7	19	93.6	1	N/A
Outer nasal	103.0 ± 41.5	12	97.9 ± 30.2	8	.758
Outer inferior	130.4 ± 28.2	9	130.4 ± 46.9	11	.621

All values are presented as mean ± standard deviation.

[a]Center = within 0.5 mm from the foveal center; Inner = 0.5–1.5 mm from the foveal center; Outer = 1.5–3.0 mm from the foveal center; Whole = within 3.0 mm from the foveal center.

[b]Mann–Whitney *U* test.

SDC

SENSITIVITY AND SPECIFICITY OF DETECTING RETICULAR PSEUDODRUSEN IN MULTIMODAL IMAGING IN JAPANESE PATIENTS

NAOKO UEDA-ARAKAWA, MD, SOTARO OOTO, MD, AKITAKA TSUJIKAWA, MD, KENJI YAMASHIRO, MD, AKIO OISHI, MD, NAGAHISA YOSHIMURA, MD

Purpose: To identify reticular pseudodrusen (RPD) in age-related macular degeneration using multiple imaging modalities, including the blue channel image of fundus photography, infrared reflectance (IR), fundus autofluorescence, near-infrared fundus autofluorescence, confocal blue reflectance, indocyanine green angiography, and spectral-domain optical coherence tomography (SD-OCT), and to compare the sensitivities and specificities of these modalities for detecting RPD.

Methods: This study included 220 eyes from 114 patients with newly diagnosed age-related macular degeneration. Patients underwent fundus photography, IR, fundus autofluorescence, near-infrared fundus autofluorescence, confocal blue reflectance, indocyanine green angiography, and SD-OCT in both eyes. Eyes were diagnosed with RPD if they showed reticular patterns on at least two of the seven imaging modalities.

Results: Thirty-seven eyes were diagnosed with RPD. However, SD-OCT and IR had the highest sensitivity (94.6%), and at the same time, SD-OCT had a high specificity (98.4%). The blue channel of color fundus photography, confocal blue reflectance, and indocyanine green angiography had a specificity of 100% but had lower sensitivity than that of SD-OCT and IR.

Conclusion: For detecting RPD, IR and SD-OCT had the highest sensitivity. Although SD-OCT had the highest sensitivity and specificity, RPD detection should be confirmed using more than one modality for increased accuracy.

RETINA 33:490–497, 2013

Reticular drusen were first identified as a peculiar yellowish pattern in the macula of patients with age-related macular degeneration (AMD) using blue light fundus photography.[1] Arnold et al[2] described a yellowish interlacing network of oval or round lesions termed reticular pseudodrusen (RPD) with a diameter of 125 μm to 250 μm visible on red-free fundus photography or infrared scanning laser ophthalmoscopy (SLO). Recently, reticular drusen and RPD have been recognized as an additional distinctive morphologic feature observed in AMD.[3] Several reports have suggested that RPD are associated with a high risk of progression to exudative AMD and geographic atrophy (GA).[4–6]

The development of new imaging modalities, such as confocal SLO and spectral-domain optical coherence tomography (SD-OCT), has led to improvements in the diagnosis of RPD.[3,7,8] Lois et al[9] used confocal SLO fundus autofluorescence (FAF) imaging for patients with early AMD and defined the term "reticular pattern of FAF" as small, ill-defined areas of decreased FAF surrounded by areas of increased FAF signal. Schmitz-Valckenberg et al[6] reported that it was easier to identify RPD in eyes with GA secondary to AMD using confocal SLO imaging technology, especially infrared reflectance (IR) and FAF, rather than conventional

From the Department of Ophthalmology and Visual Sciences, Kyoto University Graduate School of Medicine, Kyoto, Japan.

The authors have no financial interests or conflicts of interest.

Supplemental digital content is available for this article. Direct URL citations appear in the printed text and are provided in the HTML and PDF versions of this article on the journal's Web site (www.retinajournal.com).

Reprint requests: Sotaro Ooto, MD, Department of Ophthalmology and Visual Sciences, Kyoto University Graduate School of Medicine, 54 Kawahara-cho, Shogoin, Sakyo-ku, Kyoto 606-8507, Japan; e-mail: ohoto@kuhp.kyoto-u.ac.jp

fundus photography. Similarly, Querques et al[10] described that RPD were far more delineated on IR image than on blue light frames of fundus photography. In eyes with late AMD, RPD were reported to be found more frequently by SD-OCT than by examining the blue channel of color fundus photography.[8] However, the identification of characteristic but subtle changes associated with RPD requires careful analysis, and other phenotypic alterations such as soft or hard drusen may interfere with RPD detection or result in false-positives. In addition, it remains unknown which modalities have the best specificity and sensitivity for RPD detection.

The purpose of this study was to determine RPD in AMD using multiple imaging methods, including conventional fundus photography, IR, FAF, near-infrared FAF (NIR-FAF), confocal blue reflectance (CBR), indocyanine green angiography (IA), and SD-OCT imaging and to compare the sensitivities and specificities for detecting RPD between these methods.

Patients and Methods

This study included 114 consecutive patients with AMD who first visited the Macula Service of the Department of Ophthalmology at the Kyoto University Hospital between January 2010 and November 2010. Subjects included in this study had one of the following conditions in at least one eye: early AMD, neovascular AMD, or GA. Early AMD was defined as the presence of soft drusen ($\geq$63 μm) or areas of hyperpigmentation or hypopigmentation in the retinal pigment epithelium (RPE), and GA was defined using color fundus photography as a sharply delineated area ($\geq$175 μm) of hypopigmentation, depigmentation, or apparent absence of the RPE in which choroidal vessels were clearly visible. Neovascular AMD was defined as neovascularization detected using fluorescein angiography or IA. To differentiate neovascular AMD from other forms of choroidal neovascularization (CNV), we excluded patients younger than 50 years old and eyes with high myopia (refractive error $<$ –6.0 diopters or axial length $>$ 26.5 mm). Eyes with other macular abnormalities, such as pathologic myopia, idiopathic CNV, presumed ocular histoplasmosis, angioid streaks, other secondary CNV, central serous chorioretinopathy, epiretinal membrane, or retinal arterial macroaneurysm, were excluded from this study. All investigations adhered to the tenets of the Declaration of Helsinki, and the current study was approved by the Institutional Review Board and the Ethics Committee of the Kyoto University Graduate School of Medicine.

Multimodal Imaging Methods

All patients underwent a complete ophthalmologic examination, including measurement of best-corrected visual acuity, determination of intraocular pressure, indirect ophthalmoscopy, slit-lamp biomicroscopy with a noncontact lens, color fundus photography, SLO, SD-OCT, fluorescein angiography, and IA in both eyes.

Color fundus photography (field 30°–40°) was acquired digitally using a Topcon TRC NW6S nonmydriatic retinal camera (Topcon, Tokyo, Japan). To examine the blue channel of the color photography, Image J software (National Institutes of Health, Bethesda, MD) was used to display the individual color channels (red, green, and blue) of the obtained photographs. In Image J software, the commands Image $>$ Color $>$ Split Channels were used and then, if needed, the commands Image $>$ Adjust $>$ Brightness/Contrast were used to obtain the best possible images.

Infrared reflectance, FAF, NIR-FAF, CBR, and IA images were acquired using a confocal SLO (Spectralis HRA + OCT; Heidelberg Engineering, Heidelberg, Germany). Infrared reflectance images were obtained using a light stimulus of 820 nm. Images of FAF were obtained using an excitation light of 488 nm and a barrier filter beginning at 500 nm, and NIR-FAF images were obtained in the IA mode (excitation: 790 nm; detection $>$800 nm). Each FAF or NIR-FAF image was compiled from an average of 15 to 20 scans by the SLO software. Images of CBR were obtained using a light stimulus of 488 nm. The field of view was set to 30° $\times$ 30° centered on the macula.

Spectral-domain optical coherence tomography was conducted using the Spectralis HRA+OCT (Heidelberg Engineering). First, horizontal and vertical line scans through the fovea center were obtained at a 30° angle, followed by serial horizontal scans with an examination field size ranging from 30° $\times$ 10° to 30° $\times$ 25°, depending on the case. At each location of interest on the retina, 50 SD-OCT images were acquired and averaged to reduce speckle noise.

Definition of Reticular Pseudodrusen Using Multimodal Imaging

All images were evaluated independently by two experienced ophthalmologists (N.U.-A. and S.O.). In case of discrepancies, a third grader (A.T.) was asked to arbitrate. In the current study, eyes were diagnosed with RPD if they showed with reticular patterns on at least two of the following: the blue channel image of color fundus photography, IR, FAF, NIR-FAF, CBR, IA, or SD-OCT. For the blue channel of contrast-enhanced

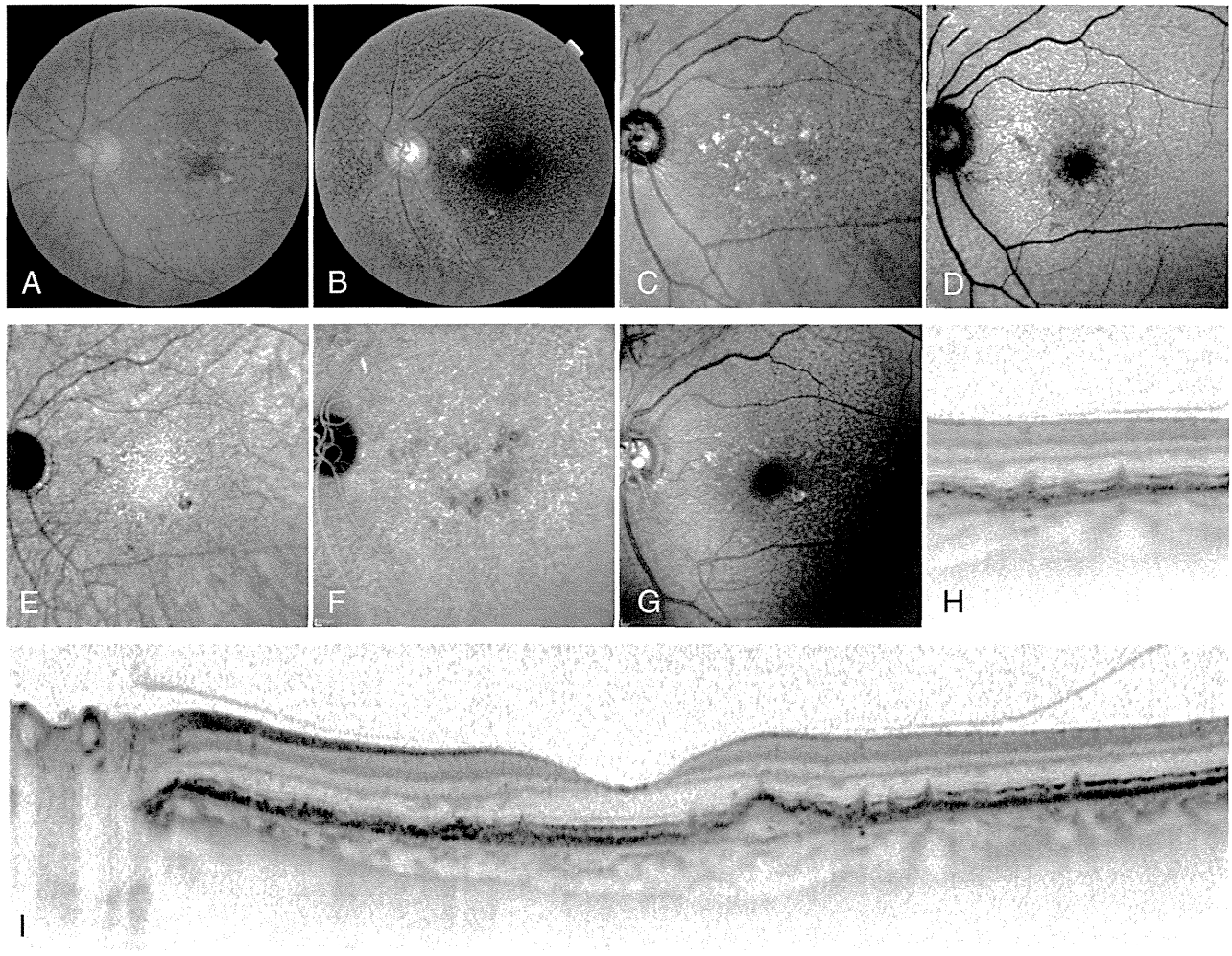

Fig. 1. Reticular patterns in multimodal imaging on an eye with early AMD. **A**. Color fundus photography. **B**. Blue channel of contrast-enhanced color fundus photography. For color fundus or the corresponding blue channel of contrast-enhanced color fundus photography, reticular pattern was identified as light interlacing networks of 125 μm to 250 μm wide. **C**. IR. Reticular IR was defined as groups of hyporeflectant lesions against a background of mild hyperreflectance with analogous characteristics. **D**. Fundus autofluorescence. Reticular FAF was defined as a grouping of ill-defined, hypofluorescent lesions against a background of mildly elevated FAF. **E**. Near-infrared fundus autofluorescence. Reticular NIR-FAF was defined as a grouping of ill-defined, hypofluorescent lesions against a background of mildly elevated NIR-FAF. **F**. Indocyanine green angiography. For IA, a reticular pattern was identified as a distinctive grouping of hypofluorescent dots present in the late phases of the angiogram. **G**. Confocal blue reflectance. Reticular pattern was identified as light interlacing networks of 125 μm to 250 μm wide. **H** and **I**. Spectral-domain optical coherence tomography. On SD-OCT, reticular lesions were defined as $\geq$5 hyperreflective mounds or triangular lesions above the RPE in $\geq$1 B scan.

color fundus photography, a reticular pattern was identified as light interlacing networks of 125 μm to 250 μm wide (Figure 1).[2] Reticular AF was characterized as a group of ill-defined, hypofluorescent lesions against a background of mildly elevated AF (Figures 1 and 2).[9,11] Reticular IR was defined as groups of hyporeflectant lesions against a background of mild hyperreflectance with analogous characteristics (Figures 1 and 2).[12] For CBR imaging, a reticular pattern was identified as light interlacing networks of 125 μm to 250 μm wide (Figure 1).[12] Reticular NIR-FAF was characterized as a group of ill-defined, hypofluorescent lesions against a background of mildly elevated NIR-FAF (Figure 1). For IA, a reticular pattern was identified as a distinctive grouping of hypofluorescent dots present in the late phases of the angiogram (Figures 1 and 2).[12,13] In SD-OCT, reticular lesions were defined as $\geq$5 hyperreflective mounds or triangular lesions above the RPE in $\geq$1 B-scan (Figures 1 and 2).[8] Only images of eligible quality were analyzed, and only eyes with eligible image quality in at least five imaging modalities were included in this study.

Statistical Analysis

Statistical analysis was performed using software designed for this purpose (SPSS 17; SPSS, Inc, Chicago, IL). All values are presented as means ± standard deviations. For statistical analysis, visual acuity

measured using a Landolt chart was converted to the logarithm of the minimum angle of resolution. Welch's *t*-test was used to compare two groups. For all analyses, $P < 0.05$ was considered statistically significant.

Results

In this study, 228 eyes from 114 consecutive patients with AMD were reviewed; however, 2 eyes were excluded because of phthisis bulbi, and 6 eyes were excluded because of poor image quality in ≥3 imaging modalities. Thus, 220 eyes from 114 patients were included in this study. Of these eyes, the number of eyes with good image quality was 220 on color fundus photography, 220 on IR, 220 on IA, 220 on SD-OCT, 217 on FAF, 204 on CBR, and 136 with NIR-FAF. The patients consist of 79 men and 35 women, aged between 52 and 92 years (mean, 73.8 ± 9.4 years). The visual acuity ranged from 0.01 to 1.5 (logarithm of the minimum angle of resolution = 0.396 ± 0.512).

On the blue channel of color fundus photography, IR, FAF, NIR-FAF, CBR, IA, or SD-OCT, a reticular pattern was found in 28 of 220 eyes (12.7%), 50 of 220 eyes (22.7%), 41 of 217 eyes (18.9%), 14 of 136 eyes (10.3%), 27 of 204 eyes (13.2%), 27 of 220 eyes (12.3%), and 38 of 220 eyes (17.3%), respectively. The interobserver concordance (kappa score) for initial grading of the reticular pattern ranged from 0.563 to 0.963 among the modalities (Table 1).

In the current study, 37 eyes in 21 patients (9 men and 12 women) had a reticular pattern according to ≥2 imaging modalities; these eyes were diagnosed with RPD. The mean age of the 21 patients with RPD was 80.4 ± 7.6 years (range, 65–92 years), which was significantly higher than that of patients without RPD (72.3 ± 9.1 years; range, 52–88 years; $P = 0.0002$, *t*-test). Of the 21 patients diagnosed with RPD, 19 patients (90.5%) had late AMD (CNV or GA) in at least 1 eye.

The number of imaging modalities that identified reticular patterns for each eye is shown in **Supplemental Digital Content 1** (see **Table 1**; http://links.lww.com/IAE/A140). Only two eyes showed reticular patterns in all imaging modalities; however, 15 eyes showed reticular patterns in 6 modalities, and all eyes showed reticular patterns in at least 3 modalities.

The specificities for the detection of RPD using the blue channel of color fundus photography, IR, FAF, NIR-FAF, CBR, IA, and SD-OCT were 100%, 91.8%, 95.0%, 95.3%, 100%, 100%, and 98.4%, respectively, whereas their sensitivities were 75.7%, 94.6%, 86.5%, 32.1%, 77.1%, 73.0%, and 94.6%, respectively (Tables 2 and 3). Overall, SD-OCT had the highest sensitivity (94.6%) and a high specificity (98.4%). Infrared reflectance also had the highest sensitivity but had a false-positive rate of 8.2%. Color fundus photography, CBR, and IA had specificities of 100% but had lower sensitivity than that of SD-OCT, IR, and FAF. Near-infrared FAF had a low sensitivity (32.1%) (Table 3). **Supplemental Digital Content 2** (see **Table 2**; http://links.lww.com/IAE/A141) shows the results by reviewing SLO images only corresponding to the area imaged by SD-OCT.

Distribution of the reticular pattern in each imaging modality can be seen in Figures 3–5. The diameter of the inner, middle, and outer circle was 1 mm, 3 mm, and 6 mm, respectively. Reticular pattern was most frequently detected in the superior outer macula in all modalities. Of the 7 modalities, only IR and SD-OCT could detect RPD within the center circle area (1-mm diameter). In addition, IR and SD-OCT could detect RPD in more subfields compared with other modalities (fundus photography, FAF, NIR-FAF, CBR, and IA) in 23 eyes (62%) and 22 eyes (59%), respectively.

Table 1. Agreement Rates and Kappa Coefficients between Two Graders

Imaging Modality	Agreement Rate (%)	Kappa Coefficient
Fundus photography*	94.7	0.895
IR	91.2	0.619
FAF	89.3	0.700
NIR-FAF	84.2	0.563
CBR	91.2	0.817
IA (late phase)	96.5	0.930
SD-OCT	98.2	0.963

*Blue channel of color fundus photography.

Table 2. Specificity for Detection of RPD

Imaging Modality	Specificity, n (%)	False-Positives, n (%)
Fundus photography*	183/183 (100)	0/183 (0)
IR	168/183 (91.8)	15/183 (8.2)
FAF	171/180 (95.0)	9/180 (5.0)
NIR-FAF	103/108 (95.3)	5/108 (4.7)
CBR	169/169 (100.0)	0/169 (0)
IA (late phase)	183/183 (100.0)	0/183 (0)
SD-OCT	180/183 (98.4)	3/183 (1.6)

*Blue channel of fundus photography.

Discussion

Reticular pseudodrusen have traditionally been identified using blue-light fundus photography; however, with the development of imaging technique, recent studies have suggested that additional methods should be used to improve the diagnostic accuracy of

Table 3. Sensitivity for Detection of RPD

Imaging Modality	RPD Detected (*n*)	Sensitivity (%)
Fundus photography*	28/37	75.7
IR	35/37	94.6
FAF	32/37	86.5
NIR-FAF	9/28	32.1
CBR	27/35	77.1
IA (late phase)	27/37	73.0
SD-OCT	35/37	94.6

*Blue channel of fundus photography.

examinations for RPD.[3,12] Sarks et al[4] suggested that FAF was the most reliable method for distinguishing RPD, and Smith et al[11] reported that FAF imaging had >90% sensitivity for identifying RPD. In a later report, they described the sensitivities of several imaging methods for detecting RPD (IA, 100%; IR, 95%; FAF, 86%; and color fundus photography, 88%).[12] Zweifel et al[7] reported that IR images revealed many more pseudodrusen than did the blue channel of color fundus photography. Schmitz-Valckenberg et al[6] reported that for the detection of RPD, confocal SLO imaging was superior to fundus photography and recommended IR and FAF imaging as optimal choices for the characterization of RPD. In each of these previous studies, multiple imaging methods were used, but RPD was deemed positive if it was detected by one imaging technique. However, the characteristic changes associated with RPD are often subtle (as seen in Figure 2); thus, identification of RPD requires careful analysis.

In the present study, seven imaging methods, namely, the blue channel of color fundus photography, IR, FAF, NIR-FAF, CBR, IA, and SD-OCT, were used for a definite diagnosis of RPD. We evaluated the specificity and sensitivity of these imaging methods.

Infrared reflectance imaging had superior sensitivity compared with that of the blue channel of color fundus photography, consistent with the results of Zweifel et al[7] and Smith et al,[12] perhaps because IR is least affected by media opacity. However, IR had the highest false-positive rate among the seven methods. On IR images, RPD are identified as a pattern-like grouping

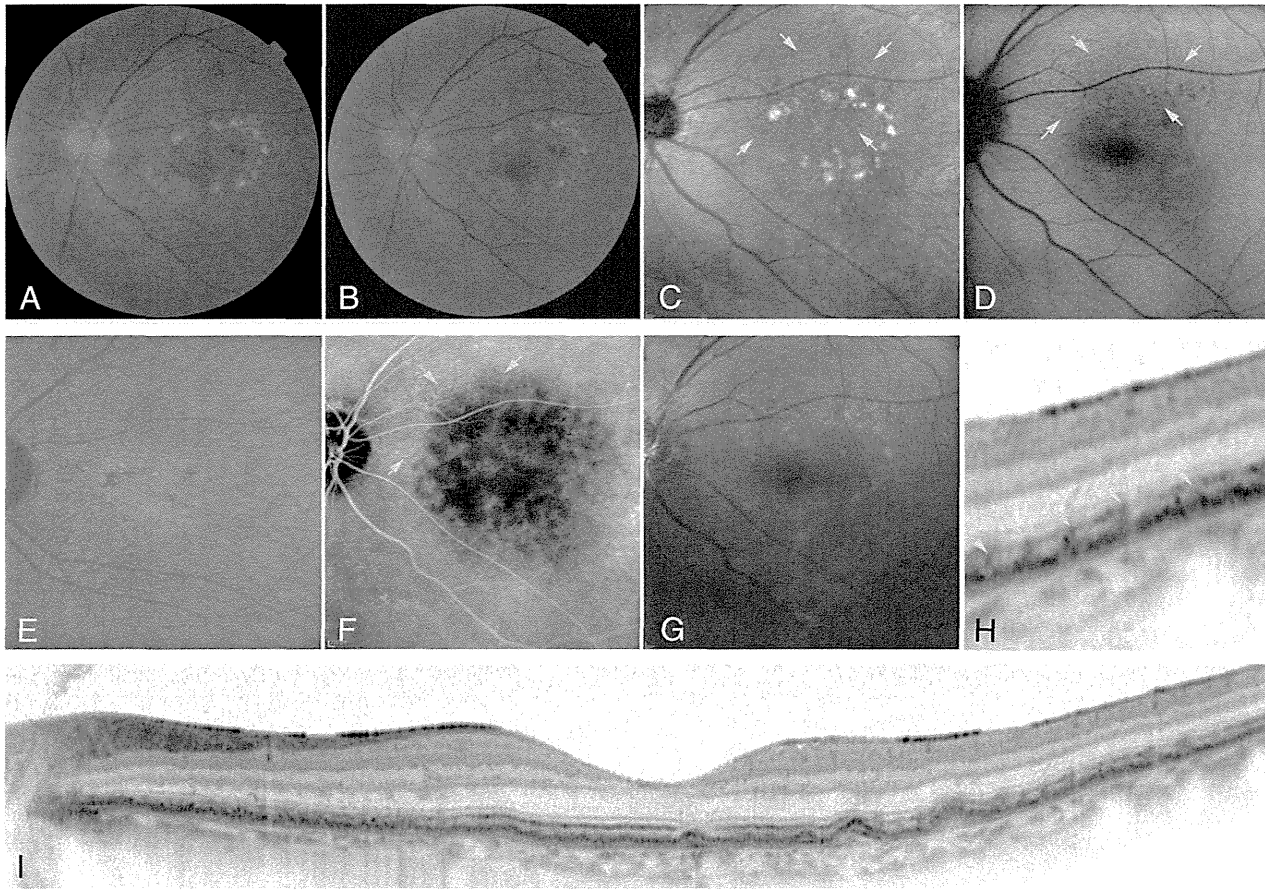

Fig. 2. Images of a patient with exudative AMD and RPD. **A**. Color fundus photography. **B**. Blue channel of contrast-enhanced color fundus photography. **C**. IR imaging. **D**. FAF imaging. **E**. NIR-FAF imaging. **F**. Late-phase IA imaging. **G**. CBR imaging. **H** and **I**. Spectral-domain optical coherence tomography. Reticular pseudodrusen are visible in IR (C), FAF (D), IA (F), and SD-OCT (H and I) images (arrows). However, RPD appears unclear in fundus photography (A and B), NIR-FAF (E), and CBR (G) images.